THE JOURNAL OF BIOLOGICAL CHEMISTRY VOL. 290, NO. 50, pp. 29808–29819, December 11, 2015

Tumor Suppressor Lzap Suppresses Wnt/β-Catenin Signaling to Promote Zebrafish Embryonic Ventral Cell Fates via the Suppression of Inhibitory Phosphorylation of Glycogen Synthase Kinase 3*[S]

Received for publication, June 4, 2015, and in revised form, October 14, 2015 Published, JBC Papers in Press, October 16, 2015, DOI 10.1074/jbc.M115.669309

Kun-Yang Lin[‡§1], Shih-Han Kao[‡], Chun-Ming Lai[‡¶], Ciao-Ting Chen[§2], Chang-Yi Wu[‖], Hwei-Jan Hsu[‡3], and Wen-Der Wang[§4]

From the [‡]Institute of Cellular and Organismic Biology, Academia Sinica, 128 Academia Road, Section 2, Nankang, Taipei 11529, Taiwan, [¶]Molecular and Biological Agricultural Sciences Program, Taiwan International Graduate Program, National Chung-Hsing University and Academia Sinica, Taipei 11529, Taiwan, [§]Department of BioAgricultural Science, National Chiayi University, Chiayi 60004, Taiwan, and [‖]Department of Biological Sciences, National Sun Yat-Sen University, Kaohsiung City 80424, Taiwan

Background: Lzap is a novel tumor suppressor.
Results: Elimination of Lzap in fish embryos or in a human tongue carcinoma cell line increases inhibitory phosphorylation of GSK3, which controls much cellular signaling, including Wnt/β-catenin signaling.
Conclusion: Lzap promotes GSK3 activity.
Significance: This introduces a new regulator of GSK3 and a potential target for cancer therapy.

Wnt/β-catenin signaling controls various cell fates in metazoan development, and its dysregulation is often associated with cancer formation. However, regulations of this signaling pathway are not completely understood. Here, we report that Lzap, a tumor suppressor, controls nuclear translocation of β-catenin. In zebrafish embryos disruption of *lzap* increases the expression of *chordin* (*chd*), which encodes a bone morphogenetic protein (BMP) antagonist that is localized in prospective dorsal cells and promotes dorsal fates. Consistently, *lzap*-deficient embryos with attenuated BMP signaling are dorsalized, which can be rescued by overexpression of zebrafish *lzap* or *bmp2b* or human *LZAP*. The expansion of *chd* expression in embryos lacking *lzap* is due to the accumulation of nuclear β-catenin in ventral cells, in which β-catenin is usually degraded. Furthermore, the activity of GSK3, a master regulator of β-catenin degradation, is suppressed in *lzap*-deficient embryos via inhibitory phosphorylation. Finally, we also report that a similar regulatory axis is also likely to be present in a human tongue carcinoma cell line, SAS. Our results reveal that Lzap is a novel regulator of GSK3 for the maintenance of ventral cell properties and may prevent carcinogenesis via the regulation of β-catenin degradation.

Embryo body plan, including dorsal-ventral patterning, is established during early development. In frog and fish, certain maternal dorsal determinants (*wnt5/11* mRNA in *Xenopus* (1, 2) and *wnt8a* mRNA in zebrafish (3)) are initially located at the vegetal pole and are subsequently transported to the future dorsal region to induce β-catenin nuclear localization. In zebrafish embryos, *wnt3a*, which is co-expressed with *wnt8a* at the gastrula margin (4), is also able to activate the maternal Wnt/β-catenin pathway (3). Downstream targets of β-catenin include *bozozok/dharma* and *fibroblast growth factors* (*fgfs*), which may act in parallel to activate transcripts involved in dorsal cell fate specification (5–7). For example, Chordin is a BMP[5] antagonist involved in the establishment of the ventral to dorsal BMP signaling gradient (8). However, the mechanisms that restrict β-catenin nuclear localization to the future dorsal side have not been fully addressed.

Wnt/β-catenin signaling is evolutionarily conserved and controls many aspects of developmental processes (9). In the absence of Wnt ligands, GSK3 binds to the scaffold protein Axin and the adenomatous polyposis coli protein to form the β-catenin destruction complex. β-Catenin is phosphorylated by GSK3 and subjected to ubiquitin-dependent degradation. The binding of Wnt to its receptors (Frizzled and lipoprotein receptor-related proteins 5 or 6 (LRP5/6)) induces the phosphorylation of LRP5/6 PPPSP*X*S motif (a cytoplasmic tail), which consequently affects the catalytic pocket of GSK3 to directly block its activity (10). Thus, β-catenin is stabilized and allowed to translocate into the nucleus, where it modulates target transcription by interacting with members of the LEF1/TCF family of transcription factors. In addition to Wnt signaling,

* This work was supported by intramural funding from the Institute of Cellular and Organismic Biology, Academia Sinica, Taiwan. The authors declare that they have no conflicts of interest with the contents of this article.
[S] This article contains supplemental Table S1 and Figs. S1–S14.
[1] Present address: Molecular and Biological Agricultural Sciences Program, Taiwan International Graduate Program, National Chung-Hsing University and Academia Sinica, Taipei 11529.
[2] Present address: Institute of Bioinformatics and Structural Biology, National Tsing-Hua University, Hsinchu 30013, Taiwan.
[3] To whom correspondence may be addressed. Tel.: 886-2-2787-1541; Fax: 886-2-2785-8059; E-mail: cohsu@gate.sinica.edu.tw.
[4] To whom correspondence may be addressed. Tel.: 886-5-2717-772; Fax: 886-5-2717-755; E-mail: wangw4@mail.ncyu.edu.tw.

[5] The abbreviations used are: BMP, bone morphogenetic protein; GSK3, glycogen synthase kinase 3; HNSCC, neck and head squamous carcinoma; hpf, hours post fertilization; MO, morpholino; PP2A, protein phosphatase 2A; NNM, normal nasal mucosal.

GSK3 activity can also be suppressed by inhibitory phosphorylation mediated by insulin-like growth signaling or lithium (11–13). In vertebrates, two genes encode GSK3 (GSK3α and GSK3β) and Axin (Axin1 and Axin2). GSK3β is known to be involved in axis formation (14), whereas Axin2 is a direct target of Wnt/β-catenin signaling and acts as a feedback negative regulator for the same pathway (15). In zebrafish, two genes code for β-catenin. Only one, β-catenin2 (encoded by *cateninb2*, *ctnnb2*), is essential for dorsal axis formation (16).

LZAP (also called CDK5Rap3 or C53) is a putative tumor suppressor gene, which is not expressed in ~30% of neck and head squamous carcinoma (HNSCC) (17); in mice, loss of *lzap* accelerates tumor xenograft growth (17). The *LZAP* gene has been highly conserved during evolution, and it encodes two L*XX*LL motifs and a putative leucine zipper domain that are responsible for protein-protein interaction and DNA-binding, respectively (18). Recent studies have shown that LZAP suppresses cell cycle progression via the activation of the p53-mediated pathway (19), decreases cellular invasion and contact growth by directly inhibiting the NF-κB signaling pathway (17), and alters cell death and proliferation by suppressing mitogen-activated protein kinase p38 MAPK (20). A role for LZAP in embryogenesis has also been reported. *lzap* homozygous knock-out mice are embryonic lethal.[6] In addition, *lzap* is maternally deposited and ubiquitously expressed in zebrafish embryos during early development, and knockdown of *lzap* results in slower cell division and delayed epibolic movement (the process by which blastomeres move from the animal pole to the vegetal pole to cover the yolk) (18). These results indicate that LZAP controls several cellular processes during development; nevertheless, it is less clear how its dysregulation causes developmental disorders and cancer formation.

In this study we further report that Lzap maintains the ventral cell fate of zebrafish embryos via GSK3. Disruption of *lzap* expression increases levels of GSK3 inhibitory phosphorylation, which in turn results in the accumulation of β-catenin nuclear localization; such accumulation causes expansion of dorsal-determining Wnt/β-catenin signaling and activation of dorsal-specifying genes in prospective ventral cells, which results in embryos becoming dorsalized. Furthermore, similar molecular expression patterns were observed in a human HNSCC line, SAS. These results are thus of relevance to many cancers in which Wnt/β-catenin signaling is elevated.

Experimental Procedures

Fish Maintenance and Breeding—The wild-type zebrafish AB strain was raised and maintained under standard laboratory conditions (22). Embryos were obtained by natural fertilization and then staged and fixed as previously described (23).

Plasmid Constructs—Total RNA was extracted from zebrafish embryos at 8 h post fertilization (hpf) or human nasal mucosal cells and converted to cDNA by reverse transcription (RT) (see details below). The coding regions of human *LZAP* and zebrafish *lzap*, *bmp2b*, *bmp4*, *bmp7a*, *noggin 1*, *chd*, *bozozok*, and *axin2* were amplified using gene-specific primers (sequences available upon request) and subcloned into the pCS2+ vector for capped mRNA synthesis or into the pGEMT-T-easy vector (Promega) for generation of antisense probes.

Morpholino and mRNA Injection—Embryos were injected at the one-cell stage. The sequences of antisense morpholino (MO) oligonucleotides (Gene Tools) and siRNA (Life Technologies) used in this study were as follows: lzap 5′-UTR MO, 5′-AAGAATTACTAAAACGACCCCATGC-3′ (note that the label of *lzap* MO in the figure represents *lzap* 5′-UTR MO); *lzap* 5′-UTR-5 mismatch MO, 5′-AACAATTAGTATAACCACCCCATCC-3′; *lzap* ATG MO, 5′-AGGGAGATTCTGGATGTTCTCCATT-3′; *chd* MO, 5′-ATCCACAGCAGCCCCTCCATCATCC-3′ (24); *gsk3α* MO, 5′-CCGCTGCCGCTCATTTCGGGTTGCA-3′ (25); *gsk3β* MO, 5′-GTTCTGGGCCGACCGGACATTTTTC-3′ (25); *lzap* splice-blocking MO, 5′-ATGTTATTGTTTTACCTCCATTGCA-3′; *ctnnb2* MO, 5′-CCTTTAGCCTGAGCGACTTCCAAAC-3′ (16); control MO, 5′-CCGACTGCTGAAAGATTCGGTCGAT-3′; control siRNA, 5′-UUCCUCUCCACGCGCAGUACAUUUA-3′; *lzap* siRNA1, 5′-UGGCAAGAGAUAGUGUCCAUGUAUG-3′; *lzap siRNA2*, 5′-CAGCCUUAAGGAAGCAGGUGUCUAA-3′. Capped mRNA from the coding region of *lzap*, *bmp2b*, *gfp*, or human *LZAP* with or without *lzap* 5′-UTR MO was injected into the cytoplasm of one-cell stage embryos.

Whole Mount in Situ Hybridization and Immunochemistry—Whole mount *in situ* hybridization was performed as described (26). Antisense probes labeled with digoxigenin-UTP (Roche Applied Science) were synthesized using cDNA encoding *axin2* (5), *bmp2b* (27), *bmp4* (28), *bmp7a* (29), *chd* (30), *noggin1* (31), or *bozozok* (7) with AmpliCap™ SP6/T7 High Yield Message Maker kit (Epicenter). Digoxigenin-labeling probes were color-stained with NBT/BCIP (nitro blue tetrazolium/5-bromo-4-chloro-3-indolyl phosphate) or BM purple (only used for *bmp2b* probes) (Roche Applied Science). Immunostaining for embryos was performed as previously described (32). The following primary antibodies were used: mouse anti-β-catenin antibody (Sigma catalog #C7207, 1:250), rabbit anti-phospho-Smad antibody (Cell Signaling, catalog #9511, 1:200), rabbit anti-phospho-GSK3 (Ser-21/-9) (Cell Signaling Technology, catalog #9331, 1:2000), and rabbit anti-phospho-mitogen-activated protein kinase antibodies (Sigma, catalog #M8159, 1:500). AlexaFluor 633-conjugated goat anti-mouse and -rabbit secondary antibodies (Molecular Probes, 1:400) and AP-lined anti-rabbit secondary antibody (Cell Signaling, 1:2000) were used. Samples were stained with 0.5 μg/ml DAPI. Images were acquired using an upright fluorescence confocal microscope (Zeiss, LSM700).

PKA/C Activity Assay—PKA activities were examined by PepTag nonradioactive protein kinase assay (Promega). PKA activities are determined by the charge of phosphorylated fluorescent PepTag A1 and non-phosphorylated PepTag A1 peptides, and the charge ranges from +1 to −1 after phosphorylation. To perform the PKA activity assay, 2.5 μg of protein extracts of sphere-stage embryos were used. Bands were detected and photographed using UV light, and the fluorescence intensity of phosphorylated, compared with non-phosphorylated, peptides was quantified using an ELISA reader.

PP2 Activity Assay—Protein Phosphatase 2 activities were examined by the nonradioactive serine/threonine phosphatase

[6] W. G. Yarbrough, unpublished results.

assay system (Promega). In brief, 1 μg of protein extracts of sphere-stage embryos were used for each of protein phosphatases (PP) PP2A, PP2B, and PP2C activity assays. Embryos were homogenized in the buffers specific for PP2A, PP2B, and PP2C (33–35). After centrifugation, the supernatant was further passed through a Sephadex G-25 resin column to remove free phosphates. The eluants were used to detect the activity by the measurement of released phosphate amount from phospho-peptide (RRA(pT)VA) according to the manufacturer's instruction.

Cell Culture and Plasmid Transfection—Human embryonic kidney 293T, SAS, TW-01 (a nasopharyngeal cancer NPC cell line), and NNM (normal nasal mucosal) cells were cultured in Dulbecco's modified Eagle's medium (DMEM) with L-glutamine (Life Technologies) and 10% fetal bovine serum (FBS; 15% FBS was for NNM) plus 1% penicillin-streptomycin in a 5% CO_2 incubator.

Lentiviruses (pLenti-GIII-CMV) containing human *LZAP* BC009957 (Abm, catalog #LV114458), human *shLZAP* (small hairpin targeted *LZAP-1: TRCN0000330497*, 5′-GCAGGAGATTATAGCTCTGTA-3′; *shLZAP-2*: *TRCN0000330498*, 5′-CCCTCACTGAAGAAGCAGATT-3′) (note that *shLZAP-2* transfection causes cell death) (Taiwan National RNAi Core Facility (TNRCF) or the empty vector control (pLenti-GIII-CMV-GFP, Abm, catalog #LV459875 or pLenti-GIII-CMV-RFP, TNRCF) were used to infect cells. For lentiviral infection, 4×10^5 cells were seeded in the wells of 6-well dishes and incubated for 24 h. Lentiviral infection was performed by the addition of 10% (v/v) of lentivirus-containing medium with Polybrene (16 μg/ml) to the cell culture, which was then incubated for 24 h; transduced cells were selected by incubation with puromycin (1 μg/ml, Sigma).

For cycloheximide treatment, 3×10^5 SAS cells, SAS cells transfected with empty control vectors or LZAP were seeded in each well for 24 h. Cells were then treated with 200 μg/ml cycloheximide (Sigma) and harvested at various times. When indicated, 10 μM MG132 (Sigma) was added.

Western Blot—Immunoblot analysis was performed as previously described (36). 50 sphere stage embryos were deyolked in cold PBS by gentle pipetting. Deyolked embryos were lysed in 150 μl of sucrose lysis buffer (300 mM sucrose, 3 mM $CaCl_2$, 2 mM $MgAc_2$, 0.1 mM EDTA, 0.4% Nonidet P-40) containing freshly diluted phosphatase and protease inhibitors (1 mM DTT, 0.1 mM PMSF, 50 mM NaF with complete protease inhibitor mixture (Roche Applied Science) by pipetting and left on ice for 20 min. Cells were lysed by radioimmune precipitation lysis buffer (50 mM Tris-HCl, 150 mM NaCl, 0.1% SDS, 0.5% sodium deoxycholate, 1% Nonidet P-40) containing freshly diluted phosphatase and protease inhibitors (as described above). The following primary antibodies were used: rabbit anit-CDK5RAP3 (BETHYL, catalog #A300-871A), mouse anti-β-catenin (Sigma, catalog #C7207, 1:1000), rabbit anti-phospho-GSK3 (Ser-21/-9) (Cell Signaling Technology, catalog #9331, 1: 2000), rabbit anti-phospho-ERK1/2 (Thr-202/Th-r204) (Cell Signaling Technology, catalog #4370, 1: 2000), rabbit anti-α tubulin (Millipore, catalog #05-829), mouse anti-cyclin D1 (Santa Cruz Biotechnology, catalog #sc-8396), rabbit anti-ERK1/2 (Cell Signaling Technology, catalog #4695, 1:1000), mouse anti-GSK3 (Santa Cruz Biotechnology, catalog #sc-7291, 1:200), rabbit anti-phospho-Akt (Cell Signaling Technology, catalog #4060, 1:500), and rabbit anti-histone H3 (Abcam, catalog #ab1791, 1:1000). The following secondary antibodies were used: horseradish peroxidase (HRP)-conjugated goat anti-rabbit IgG (Jackson ImmunoResearch, 1:10,000) and HRP-conjugated goat-anti-mouse IgG (Merck Millipore, 1:10,000). Signals were detected by chemiluminescence assays using Western Lightning™ Plus-ECL kit (PerkinElmer Life Sciences). All blots are representative of at least two experiments.

RT-PCR Analysis—Total RNA of ~30 embryos of the desired stage or $\sim 4 \times 10^6$ cells were extracted using TRIzol reagent (Invitrogen). One microgram of total RNA was used for first strand cDNA synthesis (Epicenter). For examining the transcript variants of *lzap* in embryos injected with *lzap* splice-blocking MO, we performed RT-PCR (see supplemental Fig. 2). For examining expression levels of transcripts, real time quantitative real-time PCR was performed with a LightCycler 480 II thermocycler (Roche Applied Science) together with the SYBR Green Master kit (Roche Applied Science) or a LightCycler 480 Probes master reagent kit (Roche Applied Science) equipped with specific hydrolysis TaqMan probes. Gene expression data for each individual group were normalized to the expression level of *actin* (for embryos) or *GAPDH* (for cells). Results were analyzed using a previously described formula (37). The sequence of primers (and probe number) used for RT-PCR, SYBR Green, or TaqMan Real Time PCR are available up request.

Results

Lzap Controls Dorsal-Ventral Patterning—Although Lzap was first identified as a novel tumor suppressor (17), it also plays critical roles during development (18). Knock-out of *lzap* in mice is embryonic lethal, and translational knockdown of *lzap* in zebrafish embryos using two independent *lzap* morpholinos causes epibolic movement delay (18). Interestingly, although ventral and dorsal genes were shown to be expressed in *lzap* morpholinos by Liu *et al.* (Ref. 18), a closer examination of these previously published figures reveals that the expression territories of ventral genes are reduced and dorsal gene expression areas are enhanced as compared with those of control embryos, suggesting a dorsal-ventral patterning defect in *lzap* morphants. Thus, to investigate the molecular mechanisms by which disruptions in tumor suppressor genes cause developmental defects and cancer growth, we carefully examined the role of Lzap during development using zebrafish embryos as a model; zebrafish are particularly advantageous on account of their rapid external growth and amenability to genetic manipulation (38). In agreement with a previous report (18), the application of one of the reported *lzap* MOs, 5′-UTR MO (4 ng), delayed epibolic movement in 78% ±17 of embryos at 8 hpf ($n = 1539$). Furthermore, 63% ± 14 of the surviving embryos at this stage were dead at 24 hpf (supplemental Fig. S1 and Table S1). Strikingly, the remaining embryos exhibited dorsalized phenotypes as compared with wild-type embryos or embryos injected with control MO (Fig. 1 and supplemental Table S1) when analyzed at 30 hpf. Based on the degrees of dorsalization

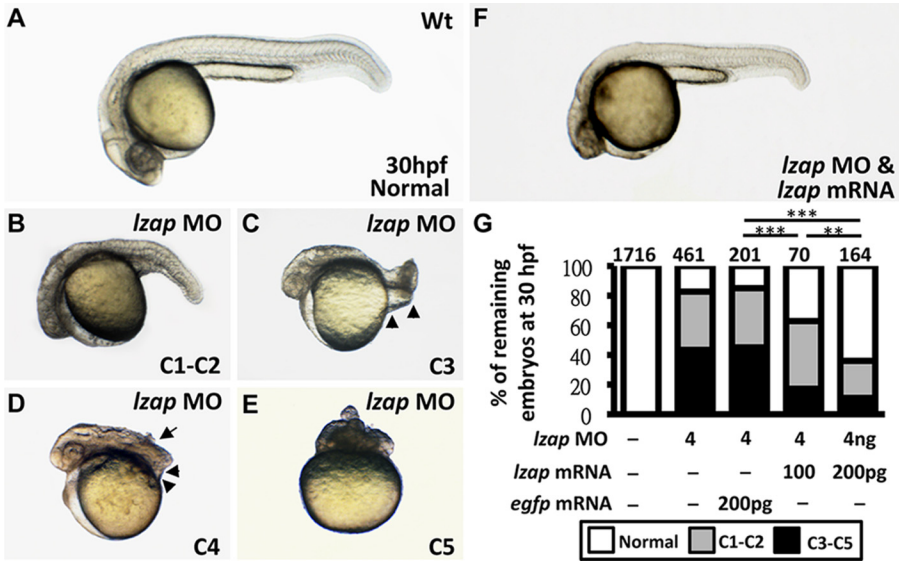

FIGURE 1. **Elimination of *lzap* causes dorsalization of embryos**. *A–E*, lateral views of 30-hpf live embryos without MO injection (wild type (*WT*)) (*A*) injected with *lzap* 5′-UTR MO (*B–E*), or coinjected with *lzap* 5′-UTR MO and *lzap* mRNA (*F*) exhibiting varying severities of dorsalized phenotypes, and categorized as Class (*C*) 1 through 5 (Mullins *et al.* (39); Kishimoto *et al.* (27)). *C1-C2* represents ventral fin loss, C3 embryos display normal but shortened trunk and yolk extension and a tail that curves upwards, C4 embryos have an abnormal body axis accompanied by a twisted tail and nearly no yolk extension, and C5 is the most severely dorsalized phenotype, characterized by the almost complete absence of posterior and ventral structures. *Arrowheads* represent the length of the yolk extension; the *arrow* points to the twisted tail. *G*, percentage of surviving embryos displaying normal, mildly dorsalized (*C1-C2*), and severely dorsalized (*C3-C5*) phenotypes in 30-hpf embryos injected with the indicated constructs. Numbers of total analyzed embryos from three individual experiments are shown *above each bar*. **, $p < 0.01$; ***, $p < 0.001$ represent the significant difference between two groups as indicated, analyzed by the χ^2 test.

(27, 39), the morphants could be categorized into five classes. Compared with those of wild-type embryos (Fig. 1*A*), the ventral tail fins of Class 1 and 2 embryos were partially lost (Class 1) or entirely absent with a smaller posterior trunk and shortened yolk extension (Class 2) (Fig. 1*B*). Class 3 and 4 embryos had a visible head structure but a shortened tail that curved upwards (Class 3) or a trunk axis twisted around itself (Class 4) (Fig. 1, *C* and *D*). Class 5 embryos had undistinguishable tissue structures on top of the yolk ball (Fig. 1*E*). After injection with 4 ng of *lzap* 5′-UTR MO, 43 and 39% of surviving *lzap* morphants ($n = 381$) exhibited mild (Class 1–2) and severe (Class 3–5) dorsalized phenotypes (Fig. 1*G*), respectively. Consistently, application of another reported morpholino, the *lzap* ATG MO, also resulted in typically dorsalized embryos (supplemental Fig. S2 and Table S1) (note that embryos injected with *lzap* ATG MO caused less obvious epibolic delay). In addition, embryos injected with two different *lzap* siRNAs also showed dorsalized phenotype (supplemental Fig. S3).

We further examined the specificity of *lzap* 5′-UTR MO on dorsalized phenotypes by supplying the *lzap*-deficient embryos with exogenous *lzap* mRNA that only covers the coding region and thereby cannot be targeted by *lzap* 5′-UTR MO (Fig. 1, *F* and *G*, and supplemental Table S1). Our results showed that the ratio of *lzap* 5′-UTR MO-induced dorsalized embryos was markedly reduced by co-injection of *lzap* mRNA in a dosage-dependent manner as compared with embryos injected with *lzap* 5′-UTR MO alone or co-injected with *lzap* 5′-UTR MO and *gfp* mRNA. However, overexpression of *lzap* mRNA did not result in ventralized embryos (supplemental Fig. S4). Furthermore, the dorsalized phenotype could also be partially rescued by co-injection of human *LZAP* mRNA (supplemental Table S1). These results indicate that Lzap controls dorsal-ventral patterning and suggest a conserved function of Lzap during development among species.

To investigate whether maternal or zygotic Lzap contributes to dorsal-ventral patterning, we used a *lzap* splice-blocking MO, which targets the junction between exon 1 and intron 1 of *lzap* and thereby affects zygotic *lzap* RNA splicing (supplemental Fig. S5, *A–C*). However, altered *lzap* RNA splicing was only observed in embryos injected with *lzap* splice-blocking MO after 8 hpf (supplemental Fig. S5*A*), and <4% of embryos injected with *lzap* splice-blocking MO ($n = 410$) exhibited dorsalized phenotypes (supplemental Fig. S5*D* and Table S1). These results indicate that maternal *lzap* has a dominant effect on early dorsal-ventral patterning.

BMP Signaling Activity Is Decreased in lzap Morphants—The BMP-Chordin axis is critical for dorsal-ventral patterning across species (2, 3, 40). BMPs are highly expressed in the ventral region and form a ventral to dorsal activity gradient, which arises mainly because of a dorsal to ventral gradient of their antagonists, such as Chordin. To determine whether *lzap* controls dorsal-ventral patterning via the BMP-Chordin axis, we first examined the expression of *bmp2b*, *bmp7a*, *bmp4*, *chd*, and *noggin 1* (encoding another BMP antagonist (41) at the 75% epiboly stage (~8 hpf) (Fig. 2, *A–H*). In stage-matched *lzap* 5′-UTR MO-injected embryos, expression territories of *bmp2b* and *bmp7a* were decreased, whereas *chd* and *noggin 1* expression regions were expanded as compared with wild-type embryos. Coincidently, quantitative PCR results revealed that expression levels of *bmp2b*, *bmp7a*, and *bmp4* were decreased, but *chd* expression was increased in *lzap* 5′-UTR MO-injected embryos at the 75% epiboly stage as compared with wild-type embryos (Fig. 2*I*). To examine whether changes in *bmps*, *chd*, and *noggin1* expression are associated with abnormal BMP sig-

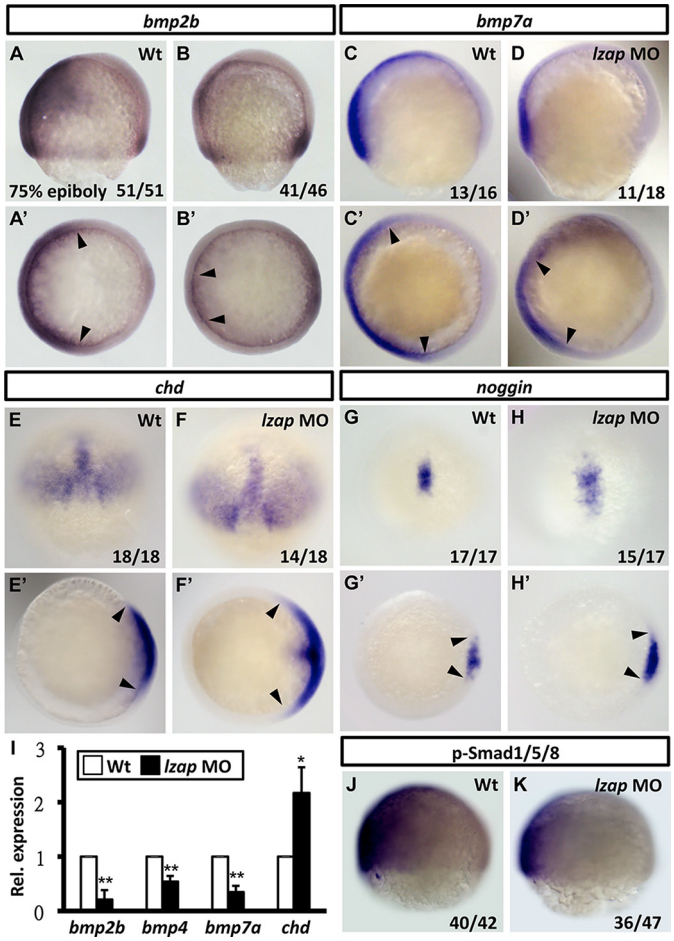

FIGURE 2. **BMP signaling activity is decreased in *lzap* morphants.** *A–H*, expression domains of *bmp2b* (*A* and *B*) and *bmp7* (*C* and *D*) are reduced in *lzap* morphants, whereas those of *chd* (*E* and *F*) and *noggin* (*G* and *H*) are expanded in *lzap* morphants (*MO*) at the 75% epiboly stage. *I*, quantitative PCR analysis of the relative expression levels of the various *bmp* mRNAs and *chd* mRNA in WT and stage-matched *lzap* morphants at the 75% epiboly stage. *Error bars* represent S.D. *, $p < 0.05$; **, $p < 0.01$. *J* and *K*, the phospho-Smad1/5/8 (p-Smad)-positive domain, which represents active BMP signaling, is decreased in *lzap* morphants at the 75% epiboly stage. *A*, *C*, *E*, *G*, and *J* are WT controls, and *B*, *D*, *F*, *H*, and *K* are stage-matched *lzap* morphants. Lateral views are seen in *A–D*, and animal views are seen in *A′–H′*, dorsal side to the *right*. Dorsal views are seen in *E–H*. *Arrowheads* in *A′–H′* point to the limits of the signal-positive expression domain. The fraction of embryos displaying the corresponding phenotype is provided in each panel. All morphants were injected with 4 ng *lzap* 5′-UTR MO.

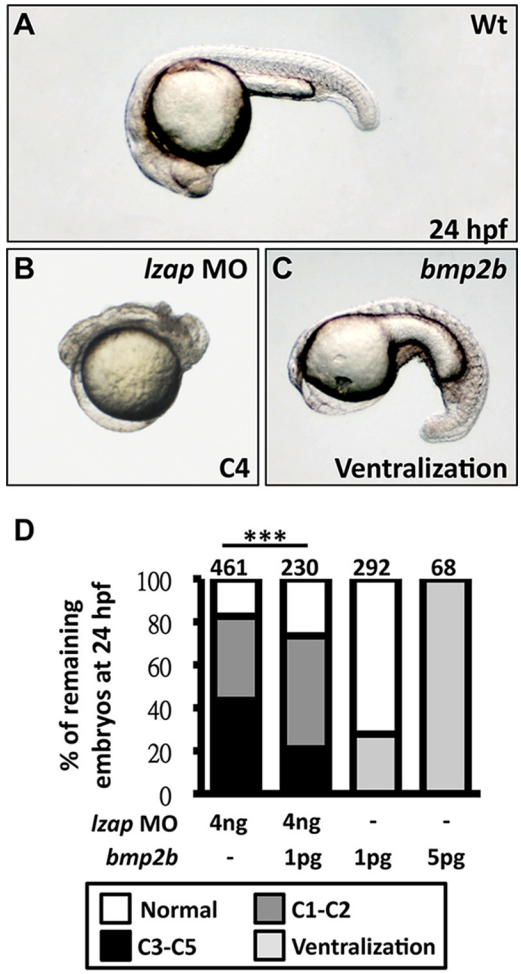

FIGURE 3. **Overexpression of *bmp2b* rescues dorsalized phenotypes in *lzap*-diminished embryos**. *A–C*, lateral views of embryos at 24 hpf. Uninjected (WT) embryos (*A*), embryos injected with *lzap* 5′-UTR morpholino (MO) (*B*), and embryos overexpressing *bmp2b* (*C*) exhibit normal, C4 snailhouse dorsalization, and ventralization, respectively. *D*, percentage of embryos exhibiting dorsalized or ventralized phenotypes at 30 hpf. Numbers of analyzed embryos are shown *above each bar*. ***, $p < 0.001$ represents the significant difference between two groups as indicated, analyzed by the χ^2 test. Data for *lzap* 5′-UTR MO-injected embryos are the same as shown in Fig. 1*F*.

naling, we used immunostaining to monitor levels of phosphorylated Smad1/5/8 proteins, which act downstream of activated BMP receptors (42). Our results indicate that the expression domain of phosphorylated Smad1/5/8 was clearly decreased in *lzap*-knockdown embryos at the 75% epiboly stage as compared with wild-type (Fig. 2, *J* and *K*), indicating a decrease of BMP signaling in *lzap*5′-UTR MO-injected embryos.

Lzap Controls Dorsal-Ventral Patterning by Maintaining BMP Signaling—To determine if the decrease of BMP signaling causes dorsalization of *lzap* morphants, we co-injected embryos with *lzap*5′-UTR MO and *bmp2b* mRNA (Fig. 3 and supplemental Table S1). As compared with wild-type embryos and dorsalized *lzap* morphants (Fig. 3, *A*, *B*, and *D*), embryos injected with *bmp2b* mRNA alone exhibited severe ventralization phenotypes at 30 hpf (Fig. 3, *C* and *D*), indicating that overexpression of *bmp2b* mRNA sufficiently increased BMP signaling. Overexpression of *bmp2b* mRNA suppressed the dorsalization phenotype of *lzap* morphants, as compared with embryos injected with *lzap*5′-UTR MO alone (Fig. 3*F*), indicating that Lzap maintains BMP signaling to control dorsal-ventral patterning.

Lzap Restricts chd Expression to the Dorsal Region before Establishment of the BMP Signaling Gradient—The BMP signaling gradient in embryos is shaped by BMP antagonists (3). In zebrafish embryos, *bmp2b* and *bmp7a* are initially ubiquitously expressed, and dorsal determinants (Wnt/β-catenin signaling) are actively induced to stimulate *chd* expression, thus creating BMP gradients at a later stage (30% epiboly stage) (6, 43, 44). To investigate how the BMP signaling gradient was affected in *lzap*-knockdown embryos, we further analyzed expression of *bmp2b* and *chd* at the sphere stage (4 hpf). We observed that the expression level and domain of *chd* was significantly increased at the dorsal site and expanded toward the ventral region in stage-matched *lzap*5′-UTR MO-injected embryos (Fig. 4, *a* and *b*), whereas *bmp2b* expression was not affected as compared

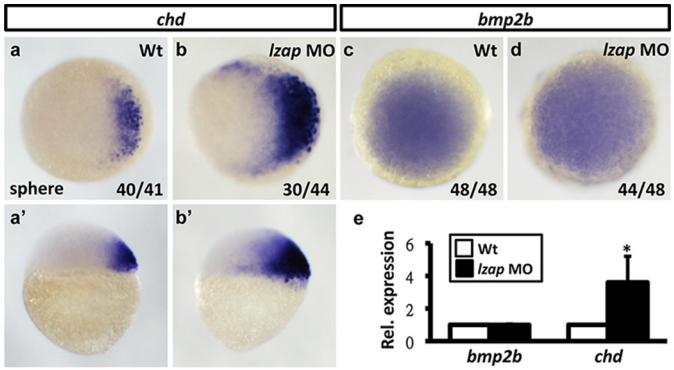

FIGURE 4. **Expression of *chd* is up-regulated before expression of *bmp2b* is decreased in *lzap*-deficient embryos.** *a–d*, expression of *chd* (*a* and *b*) and *bmp2b* (*c* and *d*) in sphere stage WT (*a* and *c*) and stage-matched *lzap* 5′-UTR MO-injected embryos (*b* and *d*). Animal views are seen in *a–d*, and lateral views are seen in *a′* and *b′*; in *a* and *b* dorsal side is to the *right*, according to expression signals. The fraction of embryos displaying the corresponding phenotype is provided in each panel. *e*, quantitative PCR analysis of relative expression levels of *bmp2b* and *chd* mRNA in WT and *lzap* morphants at the sphere stage. *Error bars* represent S.D. *, $p < 0.05$ represents the significant difference between WT and *lzap* MO-injected embryos, as analyzed by Student's *t* test. All morphants were injected with 4 ng of *lzap* 5′-UTR MO.

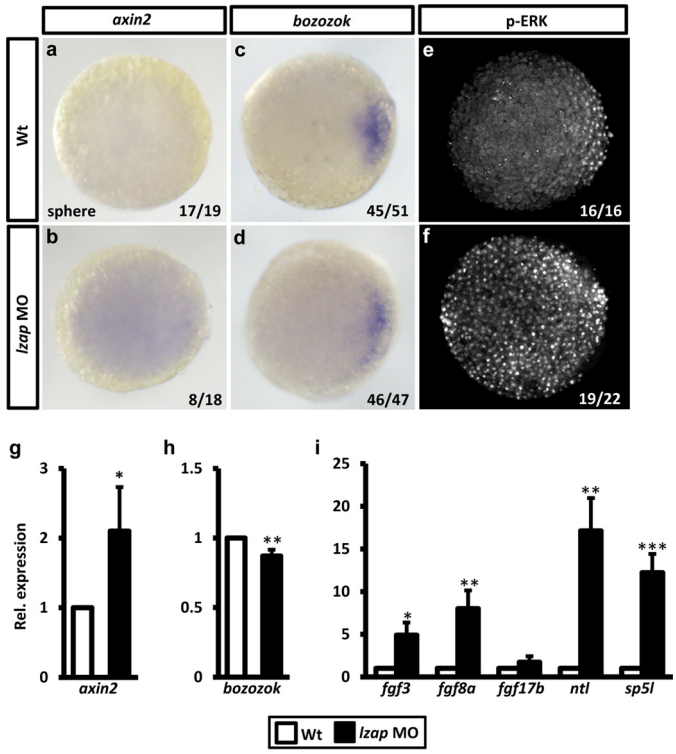

FIGURE 5. **Wnt and FGF signaling are enhanced in *lzap*-knockdown embryos.** *a–f*, detection of *axin2* (*a* and *b*) and *bozozok* (*c* and *d*) mRNA transcripts and phosphorylated p-ERK signals (*E* and *F*) in WT (*a*, *c*, and *e*) and stage-matched *lzap* 5′-UTR MO-injected embryos (*b*, *d*, and *f*) at the sphere stage. Embryos are shown as animal views; in *c–e* the dorsal side is to the right, according to expression signals. The fraction of embryos displaying the corresponding phenotype is provided in each panel. *g–i*, relative expression of *axin2* (*g*), *bozozok* (*h*), and FGF ligands and their downstream direct targets (*i*) in WT and *lzap* morphants at the sphere stage, as determined by quantitative PCR analysis. *, $p < 0.05$; **, $p < 0.01$; ***, $p < 0.001$, represent the significant difference between WT and *lzap MO*-injected embryos, as analyzed by Student's *t* test. All morphants were injected with 4 ng *lzap* 5′-UTR MO.

with controls (Fig. 4, *c* and *d*). Quantitative analysis of sphere-stage embryos also corroborated this result (Fig. 4*e*). Unexpectedly, we detected increased expression of *bmp7a* in *lzap*5′-UTR MO-injected embryos at the sphere stage (supplemental Fig. S6), suggesting a compensatory effect in response to the disruption of the BMP-Chordin gradient. Nevertheless, these results indicate that Lzap controls *chd* expression to maintain a proper gradient of BMP signaling. Furthermore, because the sphere stage occurs before the stage for epiboly initiation (dome stage, 4.3 hpf), we argue that *lzap* morphants exhibit a dorsal-ventral patterning defect in addition to the epiboly defect reported by an earlier study (18).

Wnt/β-Catenin-FGF Signaling Is Enhanced and Extended from Dorsal to Ventral in lzap Morphants—The dorsal determinant Wnt/β-catenin signaling is known to activate transcription of *fgfs* and *bozozok/dharma*, which act in parallel to control *chd* expression in the prospective dorsal region during the mid-blastula transition stage (approximately 1 h before the sphere stage) (6, 7, 45). We then examined Wnt/β-catenin signaling activity in embryos injected with *lzap*5′-UTR MO by analyzing expression of its direct target, *axin2* (which acts as a negative feedback regulator (15), at the sphere stage (Fig. 5, *a*, *b*, and *g*). Compared with control embryos, *axin2* expression was increased ~2-fold in *lzap* morphants, indicating an enhancement of Wnt/β-catenin signaling. We proceeded to analyze Fgf signaling and expression of *bozozok/dharma* and *fgfs* in *lzap* morphants at the sphere stage. Expression of *bozozok/dharma* was slightly but significantly decreased in *lzap* morphants, as compared with controls (Fig. 5, *c*, *d*, and *h*). In contrast, phosphorylated p-ERK, downstream of active Fgf signaling (6, 46), was strongly detected in nearly every cell of *lzap* morphants, as compared with the dorsally restricted p-ERK signals of wild-type embryos (Fig. 5, *e* and *f*). In addition, quantitative PCR analysis revealed increased expression of *fgf3* and *fgf8a* as well as up-regulation of FGF signaling downstream targets (47, 48), *no tail* (*ntl*) and *sp5l*, in *lzap*5′-UTR MO-injected embryos at the sphere stage (Fig. 5*i*). Although *fgf17b* has been reported to control dorsal-ventral patterning (49), no obvious changes in its expression were observed in *lzap* morphants (Fig. 5*i*). These results suggest that elevated Wnt/β-catenin-FGF signaling promotes *chd* expression in *lzap* morphants.

Lzap Suppresses Canonical Wnt/β-Catenin Signaling to Restrict chd Expression to the Dorsal Region—Upon the binding of Wnt ligands to their receptors, β-catenin translocates into the nucleus as a transcriptional co-activator to control several aspects of development, including determination of embryonic dorsal cell fate (9, 50). To determine if Lzap controls *chd* expression via Wnt/β-catenin signaling, we used quantitative PCR to examine FgF signaling and *chd* expression in embryos co-injected with *lzap* 5′-UTR MO and β-catenin2 MO (*ctnnb2* MO) at the sphere to dome stage (4–4.3 hpf) (Fig. 6, *A–F*). Consistently, expression levels of *axin2*, *fgf3*, *fgf8a*, *sp5l*, *ntl*, and *chd* were increased in embryos injected with 4 ng *lzap* 5′-UTR MO (see also Fig. 5), whereas such up-regulation was suppressed by the co-injection of *ctnnb2* MO. In addition, expression levels of these genes were also decreased in embryos injected with *ctnnb2* MO (23 ng) alone, supporting the known role of β-catenin2 in FGF signaling and *chd* expression. *In situ* hybridization results also revealed that *chd* expression level and territory were greater in *lzap* morphants, but such an increase was diminished in embryos co-injected with *lzap* 5′-UTR and

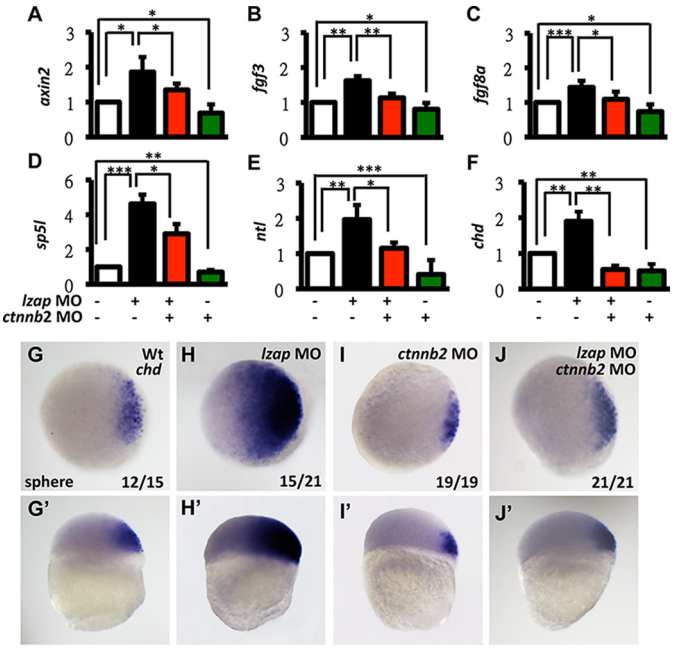

FIGURE 6. **Knockdown of *cateninb2* suppresses unregulated Wnt/FGF signaling and *chd* expression in *lzap* morphants.** *A–F*, quantitative PCR analysis of the relative mRNA expression levels of *axin2* (*A*), *fgf3* (*B*), *fgf8a* (*C*), *sp5l* (*D*), *ntl* (*E*), and *chd* (*F*) in sphere stage embryos (WT) or injected with *lzap* 5′-UTR MO and/or *ctnnb2* MO. *Error bars* represent S.D. *, $p < 0.05$; **, $p < 0.01$; ***, $p < 0.001$, represent the significant difference between WT and morpholino-injected embryos, as analyzed by Student's *t* test. Embryos were uninjected or injected with 4 ng of *lzap* 5′-UTR MO and/or 23 ng *ctnnb2* MO. *G–J*, expression of *chd* in sphere stage WT (*G*), and stage-matched embryos injected with *lzap* 5′-UTR MO (*H*), *ctnnb2* MO (*I*), or *lzap* 5′-UTR MO and *ctnnb2* MO (*J*). Animal views are seen in *G–J*, lateral views are seen in *G′* and *J′*; dorsal side to the right, according to expression signals. The fraction of embryos displaying the corresponding phenotype is provided in each panel.

ctnnb2 MO (Fig. 6, *G–J*), indicating that β-catenin2 acts downstream of Lzap to control *chd* expression.

To examine if up-regulation of Chordin expression caused dorsalization of *lzap* 5′-UTR morphants, we co-injected embryos with *lzap* 5′-UTR MO and *chd* MO (supplemental Fig. 7). Consistently, embryos injected with *lzap* 5′-UTR MO exhibited dorsalization phenotypes, whereas *chd* morphants were ventralized in a dose-dependent manner, in agreement with previous reports (24). Embryos co-injected with *lzap* 5′-UTR MO and *chd* MO are not dorsalized, but they exhibited compromised ventralization, as compared with *chd* MO morphants. This result suggests dorsalization caused by the loss of *lzap* relied on the presence of Chordin.

Lzap Suppresses Nuclear Translocation of β-Catenin via Inhibitory Phosphorylation of GSK3—We further investigated how Lzap suppresses Wnt/β-catenin signaling (Fig. 7). Immunostaining results revealed that β-catenin accumulates in the nuclei of the dorsal and marginal cells of wild-type embryos at the sphere stage (Fig. 7*A*); in contrast, strong nuclear β-catenin signals were present in cells scattered throughout *lzap* 5′-UTR-injected embryos (Fig. 7*B*). However, *ctnnb2* mRNA levels in wild-type embryos and *lzap* morphants were comparable (Fig. 7*C*), and expression levels of *wnt3a* and *wnt8a* (required for activating maternal β-catenin; Refs. 3 and 4) were decreased in *lzap* morphants as compared with the wild-type control (Fig. 7*D*). These results indicate that elimination of *lzap* may promote the stability of β-catenin independent of Wnts. Indeed, total β-catenin protein levels were increased in *lzap* morphants at the sphere stage (Fig. 7*E*), and expression of p-ERK, downstream of FGF signaling, was also consistently and dramatically increased in *lzap* morphants (supplemental Fig. 8; see also Fig. 5).

In addition to Wnt signaling (10), GSK activity can also be suppressed by inhibitory phosphorylation at serine 21 of GSK3α or serine 9 of GSK3β (p-GSK3-α/β Ser-21/-9); this results in the accumulation of β-catenin and in turn causes the dorsalized phenotype (11–13). We, therefore, hypothesized that accumulation of β-catenin in *lzap* morphants may result from the loss of GSK3β activity. To test this hypothesis, we examined GSK3 activity by subjecting embryos to Western blot with an anti-p-GSK3-α/β Ser-21/-9 antibody (Fig. 7*E*). Strikingly, inhibitory phosphorylation of GSK3 in *lzap* morphants was greatly increased as compared with that in wild-type controls at the sphere stage (Fig. 7*E*); this finding was consistent with immunostaining data (Fig. 7, *F* and *G*). Our results indicate that Lzap promotes GSK3 activity to promote the degradation of β-catenin in ventral cells via inhibitory phosphorylation.

Indeed, suppression of GSK3 expression in embryos by co-injecting *gsk3α* and *gsk3β* MO caused dorsalized phenotypes (supplemental Fig. S9), as previously described (25). The degree of dorsalizatoin was enhanced when embryos injected with *lzap* (5 ng), *gsk3α* (1 ng), and *gsk3β* (4 ng) MOs (supplemental Fig. S9), indicating a genetic interaction between LZAP and GSK3. However, knockdown of *lzap* in embryos injected with higher concentrations of *gsk3α MO* (2 ng) and *gsk3β* (6 ng) did not increase dorsalization, and overexpression of *lzap* cannot rescue dorsalization of *gsk3α* and *gsk3β* double morphants, supporting our conclusion that GSK3 acts downstream of Lzap.

Human LZAP Controls Expression of β-Catenin and Inhibitory Phosphorylation of GSK3 in Oral Cancer SAS Cells—It has been reported that LZAP is absent from ~30% of HNSCCs (17). Interestingly, we found that SAS cells, a commonly used HNSCC cell line derived from tongue carcinoma (51), exhibited similar levels of *LZAP* expression, whereas a 40% reduction of LZAP and associated with higher levels of β-catenin and inhibitory phosphorylated GSK3 (Fig. 8, *A* and *B*, and supplemental Fig. S10) as compared with NNM epithelial cells (primary culture of NNM epithelia was performed during surgery on patients with nasal polyposis) (52).

We further examined the effect of *LZAP* on GSK3 and β-catenin in human cancer cells by overexpressing *LZAP* in SAS cells. *LZAP* mRNA was increased ~1.6-fold after transfection (Fig. 8*C*), whereas LZAP protein expression was further decreased to 50% that of the original LZAP amount (Fig. 8*D*). Noticeably, similar phenomena were observed in 293T cells (supplemental Fig. S11). To determine the half-life of the LZAP protein, we first treated SAS cells with cycloheximide, an inhibitor for protein synthesis, in a time-dependent manner. Three hours after treating with cycloheximide (200 μg/ml), LZAP protein levels decreased to 30% that in SAS cells without treatment (supplemental Fig. S12). We further tested whether proteasome-dependent degradation was involved in the reduction of LZAP in *LZAP*-expressing SAS cells. To do this, SAS cells transfected with the empty control vector (as the control)

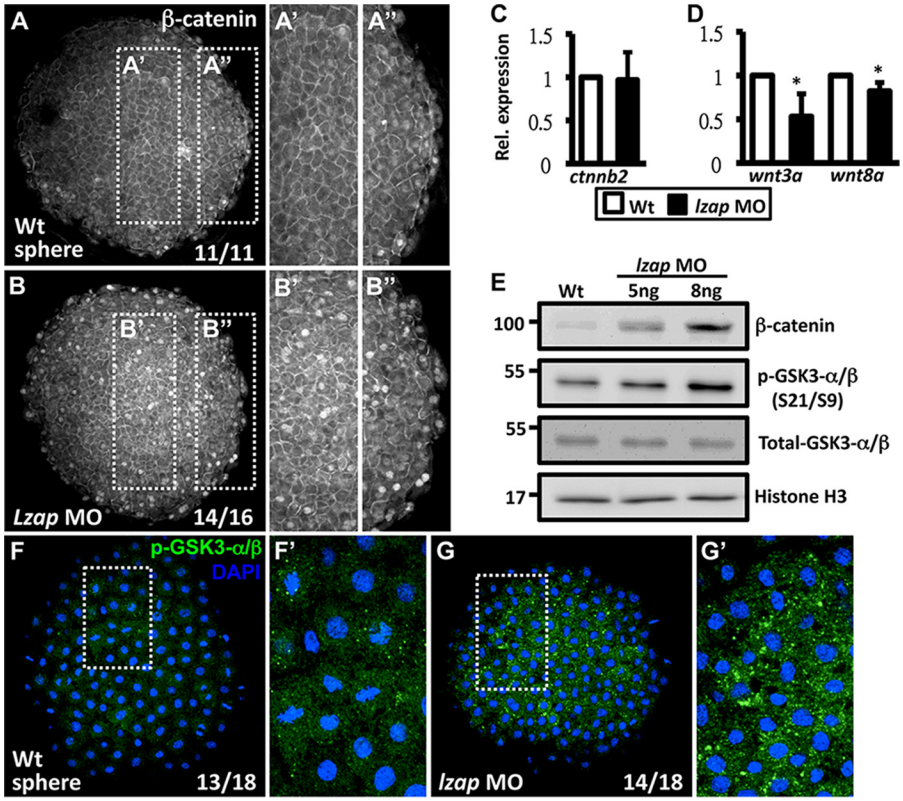

FIGURE 7. **β-Catenin nuclear localization is enhanced in *lzap* morphants via inhibitory phosphorylation of GSK3.** *A* and *B*, animal views of sphere stage WT) (*A*) and 4 ng of *lzap* 5′-UTR MO-injected embryos (*B*) labeled with β-catenin (*gray color*). In WT embryos, the dorsal side is to the *right*, according to obvious β-catenin nuclear staining. The fraction of embryos displaying the corresponding phenotype is provided in each panel. *C* and *D*, quantitative PCR analysis of relative mRNA expression levels of *ctnnb2* (*C*) and *wnt3a* and *wnt8a* (*D*) in sphere stage WT or 4 ng of *lzap* MO-injected embryos. *, $p < 0.05$ represents the significant difference between WT and morpholino-injected embryos, as analyzed by Student's *t* test. *E*, representative Western blots for β-catenin (92–97 kDa), p-ERK (44/42 kDa), and p-GSK3-α/β levels (51/46 kDa) in WT or *lzap* 5′-UTR MO-injected embryos. Histone H3 (17 kDa) was used as an internal control. Molecular weight markers are indicated to the *left of the blots*. Membranes used for detecting expression of β-catenin, p-GSK3, and histone H3 and that of p-ERK were electroblotted from replicate lanes of a single gel. *F* and *G*, animal views of sphere stage WT (*F*) and 4 ng of *lzap* 5′-UTR MO-injected embryos (*G*) labeled with Ser-21/-9 p-GSK3α/β (*green*) and DAPI (*blue*). The fraction of embryos displaying the corresponding phenotype is provided in each panel.

or *LZAP* were treated with cycloheximide (200 μg/ml) alone or co-treated with cycloheximide (200 μg/ml) and MG132 (10 μM), an inhibitor for proteasome-dependent degradation. Three hours after cycloheximide treatment, a 30% reduction of LZAP protein levels was found in control cells, whereas a 50% reduction was found in the *LZAP*-overexpressing SAS cells, indicating a fast turnover rate of LZAP in the *LZAP*-overexpressing SAS cells. Co-treatment with cycloheximide and MG132 compromised the reduction of LZAP protein in *LZAP*-overexpressing SAS cells but not in controls. LZAP protein levels in LZAP-overexpressing SAS cells were returned to ~90% of the original amount (supplemental Fig. S12). These results suggest that too many LZAP proteins induce LZAP degradation via a proteasome degradation pathway and may be an explanation for the dorsalized embryos caused by *lzap* overexpression (see supplemental Fig. S4). The decrease of LZAP protein in *LZAP*-overexpressing SAS cells was accompanied by further enhancement of inhibitory phosphorylation of GSK3 and levels of β-catenin and cyclin D1 (a direct target of Wnt/β-catenin signaling (53) (Fig. 8*D*) as compared with levels in SAS cells transfected with the empty control vector. These results indicate that LZAP may also maintain tissue homeostasis via regulation of Wnt/β-catenin signaling, as a similar mechanism was observed in zebrafish embryos. Surprisingly, strengthened reduction of LZAP in SAS cells by *shRNAi* still increased levels of inhibitory phosphorylated GSK3, but β-catenin and cyclin D1 expressions were decreased (Fig. 8*E*). Knockdown *LZAP* in 293T by *shRNAi* also showed a similar result (supplemental Fig. S13). These results indicate a complex regulation of LZAP on Wnt/β-catenin signaling pathways. Nevertheless, our results strongly argue that LZAP is a novel dual regulator of GSK3 in fish and human cell lines.

Discussion

Wnt/β-catenin signaling promotes dorsal cell fates in frogs and fish, and it is also hyperactivated in several types of cancer (54, 55); however, its regulation remains incompletely understood. Here, we report that LZAP, a tumor suppressor, regulates Wnt/β-catenin signaling via the suppression of inhibitory phosphorylation of GSK3 in fish embryos and in cancer (Fig. 9). Within prospective dorsal cells of zebrafish embryos, maternal Wnt proteins activate their receptor, Frizzled, which directly inhibits GSK3 activity (54), allowing nuclear translocation of β-catenin. In contrast, within prospective ventral cells, GSK3 retains its activity, at least in part through Lzap, and this results in the degradation of β-catenin. Note that Lzap in dorsal cells may control GSK3 activity via a similar mechanism because *chd* expression is dramatically increased in the dorsal cells of *lzap*-

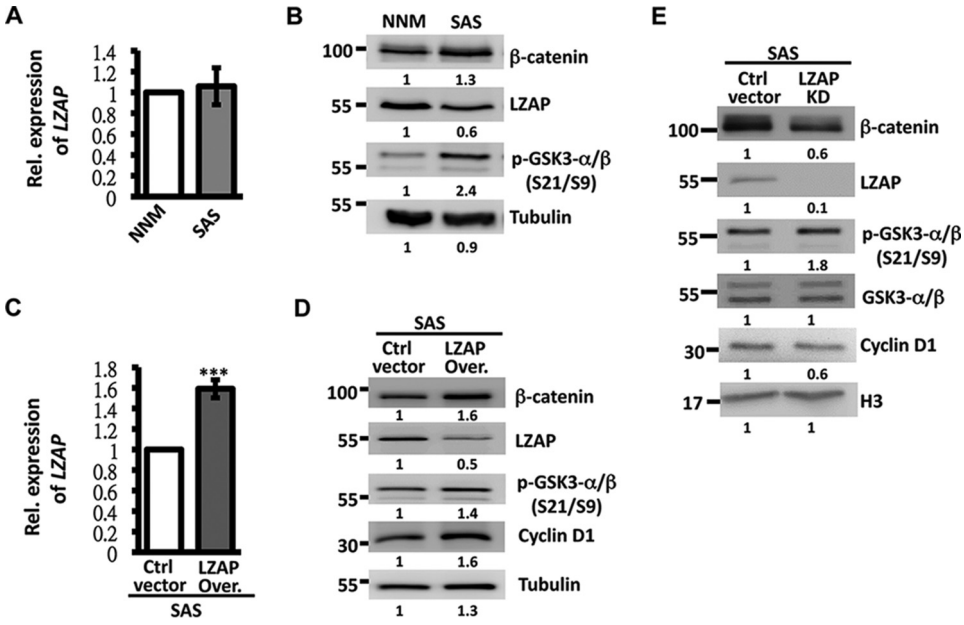

FIGURE 8. **Human LZAP promotes β-catenin degradation and GSK3 activity in SAS cells.** *A*, expression levels of *LZAP* mRNA in NNM (control) and SAS cells are comparable. *B*, representative Western blots for LZAP (57 *k*Da), β-catenin (92–97 kDa), and p-GSK3-α/β levels (51/46 kDa) in NNM control or SAS cancer cells. α-Tubulin (48 kDa) was used as an internal control. Molecular weight markers are indicated to the *left of the blots*. The numbers shown *below the bands* indicate quantitative measurements of the -fold change with respect to the NNM control cells. *C*, expression levels of *LZAP* mRNA in SAS cells transfected with lentivirus containing *LZAP* or empty vector. ***, $p > 0.001$. *Over.*, overexpressing. *D* and *E*, representative Western blots for LZAP, β-catenin, p-GSK3-α/β, and cyclin D1 (37 kDa) levels in SAS cells transfected with the empty control vector, *LZAP* (*D*), or *LZAP* shRNA1 (*E*). α-Tubulin was used as an internal control. Molecular weight markers are indicated to the *left of the blots*. The numbers shown below the bands indicate quantitative measurements of -fold change with respect to the SAS control cells.

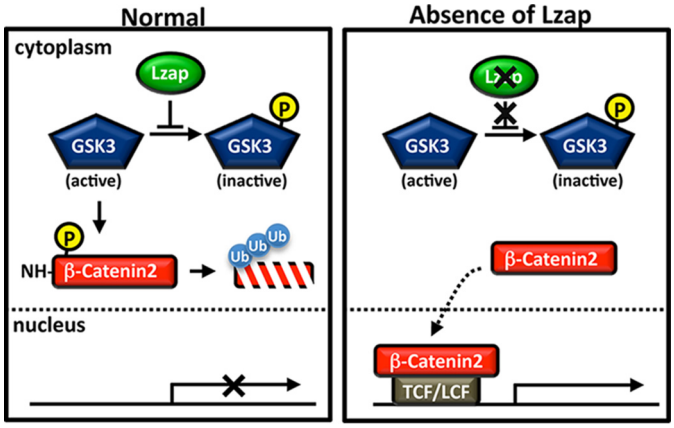

FIGURE 9. **Model of how Lzap controls β-catenin nuclear translocation.** Under normal conditions (*left panel*), Lzap suppresses the inhibitory phosphorylation of GSK3β, enabling active GSK3β to phosphorylate β-catenin for its degradation in non-dorsal zebrafish embryonic cells or normal cells. When Lzap is absent (*right panel*), inhibitory phosphorylation of GSK3β is promoted, resulting in the translocation of β-catenin into the nucleus to activate its target genes. *Ub*, ubiquitin; *TCF/LCF*, T cell factor.

deficient embryos (Fig. 4*B*). This result may also reflect the ubiquitous expression of *lzap* mRNA during early embryogenesis (18).

Lzap Controls Dorsal-Ventral Patterning in Parallel with Its Role in Epibolic Movement—Zebrafish embryos lacking *lzap* exhibit defects in both epiboly initiation and movement (18) that are dependent on cell adhesion and radial intercalation of epithelial sheets (56). Here, we further demonstrate that Lzap controls dorsal-ventral patterning by restricting Wnt/β-catenin signaling to prospective dorsal cells. Epiboly is the first morphogenetic movement of the zebrafish embryo that drives cells toward the vegetal pole (57). The initiation of epiboly involves doming of the yolk cell up into the overlying blastoderm at the dome stage (~4.3 hpf), whereas maternal β-catenin starts to accumulate in the nuclei of dorsal blastomeres as early as the 128-cell stage (~2.25 hpf) (58, 59), indicating that dorsal-ventral patterning occurs earlier than epibolic movement. Given that mutations of several genes involved in dorsal-ventral patterning (*e.g. bmp2b*) did not exhibit severe epiboly defects (60), we speculate that Lzap controls pattern formation and morphogenetic movement in a parallel manner.

Multiple Mechanisms Ensure Ventral Cell Formation—Wnt/β-catenin signaling is activated in dorsal blastomeres of frog and zebrafish embryos during early development to induce genes that determine dorsal cell fate (61). This pathway is activated by maternal Wnts that are initially located at the vegetal pole and transported to cells that will become dorsal cells. Upon binding of Wnt proteins to their receptor, Frizzled, GSK3 activity is suppressed to facilitate the nuclear localization of β-catenin. However, β-catenin and *wnt* mRNAs, including *wnt8a*, are present throughout the blastoderm (at least in zebrafish) (3, 55), suggesting that other factors are required to ensure that β-catenin only accumulates in dorsal cells. Indeed, a recent study has shown that Sfrp1 and Frzb are two maternal Wnt inhibitors that limit the spatial context of Wnt proteins in dorsal cells (3). In addition, embryos treated with inhibitors that inactivate GSK3 (required for β-catenin degradation) from the 32-cell stage to the sphere stage also result in dorsalized phenotypes (14), indicating that GSK3 activity is promoted in ventral cells to ensure ventral cell fate. It is unclear, however, how GSK3 activity in ventral cells is controlled during early embryogenesis. In this study we propose that Lzap may

enhance GSK3 activity to ensure β-catenin degradation in ventral cells.

LZAP-mediated Modulation of GSK3 Activity May Have Tumor Suppressive Effects—LZAP has been shown to interact with several proteins in the context of its anti-tumor role. For example, LZAP binds ARF (alternative reading frame) for p53 activation to suppress tumor growth (19) and, together with RelA, RCAD (regulators of C53/LZAP and DDRGK1 (DDRGK domain-containing protein 1), or NLBP (novel LZAP-binding protein) inhibits NFκB to suppress tumor invasion (17, 63, 64). However, it is not clear if LZAP plays a role in cancer cells with aberrant Wnt/β-catenin signaling.

In this study we observed that diminished Lzap expression in fish embryos suppresses GSK3 activity and causes the accumulation of β-catenin, indicating that Lzap is able to modulate GSK3 activity. In addition, levels of LZAP were decreased and accompanied by increased β-catenin and phosphorylated GSK3 in human tongue cancer SAS cells, suggesting that LZAP may control GSK3 activity to suppress tumors. Interestingly, although another HNSCC cell line, human nasopharyngeal cancer TW-01 cells, also exhibited decreased LZAP expression, β-catenin and inhibitory phosphorylation of GSK3 are decreased in this cell line (supplemental Fig. S10), indicating that the regulation of Wnt/β-catenin signaling by LZAP occurs in a cell context-specific manner.

Possible Mechanisms Underlying GSK3 Inactivation by Lzap—GSK3 functions as a downstream regulatory switch for numerous signaling pathways, including cellular responses to Wnt and insulin-like growth factor and is involved in several cellular processes, ranging from glycogen metabolism to cell proliferation as well as cell movement, apoptosis, and dorsal-ventral patterning (21, 62). Therefore, GSK3 activity is tightly regulated (62). One critical regulatory mechanism is GSK3 phosphorylation. The most important phosphorylated residues are serine 21 for GSK3α and serine 9 for GSK3β, which inhibit GSK3 kinase activity, whereas phosphorylation of tyrosine residues (Tyr-216 for GSK3β and Tyr-279 for GSK3α) is required for activation. Several kinases, including Akt, protein kinases A (PKA) and PKC, suppress GSK3 activity via phosphorylation of serine 21/-9. In contrast, protein phosphatases 1 (PP1) and 2A (PP2A) dephosphorylate the inhibitory site of GSK3, resulting in activation of GSK3. Furthermore, it has been shown that Lzap is able to interact with WIP1, a type 2C protein phosphatase (PP2C), to suppress p38 phosphorylation (20). To investigate how Lzap may control GSK3 activity, we further tested the involvement of the kinases and phosphatases described above (supplemental Fig. S14). We did not observe differences in PKA, PKB, PP2A, PP2B, or PP2C activities between wild-type and *lzap* 5′-UTR MO-injected embryos at the sphere stage. In addition, we failed to detect PKC and PP1 activities in sphere-stage embryos. Further work will be needed to dissect the molecular mechanism by which Lzap promotes.

Author Contributions—K.-Y. L., C.-Y. W., H.-J. H., and W.-D. W. designed and interpreted the experiments and wrote the paper. C.-T. C. contributed to Fig. 2. S.-H. K. and C.-M. L. contributed to Fig. 8 and supplemental Fig. S4. K.-Y. L. performed the remaining experiments.

Acknowledgments—We thank the National RNAi Core Facility Platform and the Zebrafish Core at Academia Sinica for providing reagents and zebrafish, respectively. We thank M.-Y. Liao and H.-C. Wu for providing reagents and teaching cell culture and virus infection techniques. We also thank S.-P. Hwang, R.-H. Chen, and Y.-W. Liu for valuable comments on this article and D. E. Wright for assistance with English editing.

References

1. Cha, S.-W., Tadjuidje, E., Tao, Q., Wylie, C., and Heasman, J. (2008) Wnt5a and Wnt11 interact in a maternal Dkk1-regulated fashion to activate both canonical and non-canonical signaling in *Xenopus* axis formation. *Development* **135,** 3719–3729
2. Tao, Q., Yokota, C., Puck, H., Kofron, M., Birsoy, B., Yan, D., Asashima, M., Wylie, C. C., Lin, X., and Heasman, J. (2005) Maternal Wnt11 activates the canonical wnt signaling pathway required for axis formation in *Xenopus* embryos. *Cell* **120,** 857–871
3. Lu, F.-I., Thisse, C., and Thisse, B. (2011) Identification and mechanism of regulation of the zebrafish dorsal determinant. *Proc. Natl. Acad. Sci. U.S.A.* **108,** 15876–15880
4. Shimizu, T., Bae, Y.-K., Muraoka, O., and Hibi, M. (2005) Interaction of Wnt and caudal-related genes in zebrafish posterior body formation. *Dev. Biol.* **279,** 125–141
5. Shimizu, T., Yamanaka, Y., Ryu, S. L., Hashimoto, H., Yabe, T., Hirata, T., Bae, Y. K., Hibi, M., and Hirano, T. (2000) Cooperative roles of Bozozok/Dharma and Nodal-related proteins in the formation of the dorsal organizer in zebrafish. *Mech. Dev.* **91,** 293–303
6. Ramel, M. C., and Hill, C. S. (2013) The ventral to dorsal BMP activity gradient in the early zebrafish embryo is determined by graded expression of BMP ligands. *Dev. Biol.* **378,** 170–182
7. Maegawa, S., Varga, M., and Weinberg, E. S. (2006) FGF signaling is required for β-catenin-mediated induction of the zebrafish organizer. *Development* **133,** 3265–3276
8. Sasai, Y., Lu, B., Steinbeisser, H., Geissert, D., Gont, L. K., and De Robertis, E. M. (1994) *Xenopus* chordin: a novel dorsalizing factor activated by organizer-specific homeobox genes. *Cell* **79,** 779–790
9. Clevers, H. (2006) Wnt/β-catenin signaling in development and disease. *Cell* **127,** 469–480
10. Wu, G., Huang, H., Garcia Abreu, J., and He, X. (2009) Inhibition of GSK3 phosphorylation of β-catenin via phosphorylated PPPSP*X*S motifs of Wnt coreceptor LRP6. *PLoS ONE* **4,** e4926
11. Cross, D. A., Alessi, D. R., Cohen, P., Andjelkovich, M., and Hemmings, B. A. (1995) Inhibition of glycogen synthase kinase-3 by insulin mediated by protein kinase B. *Nature* **378,** 785–789
12. McManus, E. J., Sakamoto, K., Armit, L. J., Ronaldson, L., Shpiro, N., Marquez, R., and Alessi, D. R. (2005) Role that phosphorylation of GSK3 plays in insulin and Wnt signalling defined by knockin analysis. *EMBO J.* **24,** 1571–1583
13. De Sarno, P., Li, X., and Jope, R. S. (2002) Regulation of Akt and glycogen synthase kinase-3β phosphorylation by sodium valproate and lithium. *Neuropharmacology* **43,** 1158–1164
14. Shao, M., Lin, Y., Liu, Z., Zhang, Y., Wang, L., Liu, C., and Zhang, H. (2012) GSK-3 activity is critical for the orientation of the cortical microtubules and the dorsoventral axis determination in zebrafish embryos. *PLoS ONE* **7,** e36655
15. Jho, E. H., Zhang, T., Domon, C., Joo, C. K., Freund, J. N., and Costantini, F. (2002) Wnt/β-catenin/Tcf signaling induces the transcription of Axin2, a negative regulator of the signaling pathway. *Mol. Cell. Biol.* **22,** 1172–1183
16. Bellipanni, G., Varga, M., Maegawa, S., Imai, Y., Kelly, C., Myers, A. P., Chu, F., Talbot, W. S., and Weinberg, E. S. (2006) Essential and opposing roles of zebrafish β-catenins in the formation of dorsal axial structures and neurectoderm. *Development* **133,** 1299–1309
17. Wang, J., An, H., Mayo, M. W., Baldwin, A. S., and Yarbrough, W. G. (2007) LZAP, a putative tumor suppressor, selectively inhibits NF-κB.

Cancer Cell **12,** 239–251
18. Liu, D., Wang, W. D., Melville, D. B., Cha, Y. I., Yin, Z., Issaeva, N., Knapik, E. W., and Yarbrough, W. G. (2011) Tumor suppressor Lzap regulates cell cycle progression, doming, and zebrafish epiboly. *Dev. Dyn.* **240,** 1613–1625
19. Wang, J., He, X., Luo, Y., and Yarbrough, W. G. (2006) A novel ARF-binding protein (LZAP) alters ARF regulation of HDM2. *Biochem. J.* **393,** 489–501
20. An, H., Lu, X., Liu, D., and Yarbrough, W. G. (2011) LZAP inhibits p38 MAPK (p38) phosphorylation and activity by facilitating p38 association with the wild-type p53 induced phosphatase 1 (WIP1). *PLoS ONE* **6,** e16427
21. Doble, B. W., and Woodgett, J. R. (2003) GSK-3: tricks of the trade for a multi-tasking kinase. *J. Cell Sci.* **116,** 1175–1186
22. Westerfield, M. (2000) *The Zebrafish Book: Guide for the Laboratory Use of Zebrafish (Danio rerio).* 4th Ed., University of Oregon, Eugene, Oregon
23. Kimmel, C. B., Ballard, W. W., Kimmel, S. R., Ullmann, B., and Schilling, T. F. (1995) Stages of embryonic development of the zebrafish. *Dev. Dyn.* **203,** 253–310
24. Nasevicius, A., and Ekker, S. C. (2000) Effective targeted gene "knockdown" in zebrafish. *Nat. Genet.* **26,** 216–220
25. Lee, H. C., Tsai, J. N., Liao, P. Y., Tsai, W. Y., Lin, K. Y., Chuang, C. C., Sun, C. K., Chang, W. C., and Tsai, H. J. (2007) Glycogen synthase kinase 3α and 3β have distinct functions during cardiogenesis of zebrafish embryo. *BMC Dev. Biol.* **7,** 93
26. Müller, I. I., Knapik, E. W., and Hatzopoulos, A. K. (2006) Expression of the protein related to Dan and Cerberus gene-prdc-During eye, pharyngeal arch, somite, and swim bladder development in zebrafish. *Dev. Dyn.* **235,** 2881–2888
27. Kishimoto, Y., Lee, K. H., Zon, L., Hammerschmidt, M., and Schulte-Merker, S. (1997) The molecular nature of zebrafish swirl: BMP2 function is essential during early dorsoventral patterning. *Development* **124,** 4457–4466
28. Martínez-Barberá, J. P., Toresson, H., Da Rocha, S., and Krauss, S. (1997) Cloning and expression of three members of the zebrafish Bmp family: Bmp2a, Bmp2b, and Bmp4. *Gene* **198,** 53–59
29. Schmid, B., Fürthauer, M., Connors, S. A., Trout, J., Thisse, B., Thisse, C., and Mullins, M. C. (2000) Equivalent genetic roles for bmp7/snailhouse and bmp2b/swirl in dorsoventral pattern formation. *Development* **127,** 957–967
30. Miller-Bertoglio, V. E., Fisher, S., Sánchez, A., Mullins, M. C., and Halpern, M. E. (1997) Differential regulation of chordin expression domains in mutant zebrafish. *Dev. Biol.* **192,** 537–550
31. Fürthauer, M., Thisse, B., and Thisse, C. (1999) Three different noggin genes antagonize the activity of bone morphogenetic proteins in the zebrafish embryo. *Dev. Biol.* **214,** 181–196
32. Westfall, T. A., Hjertos, B., and Slusarski, D. C. (2003) Requirement for intracellular calcium modulation in zebrafish dorsal-ventral patterning. *Dev. Biol.* **259,** 380–391
33. Liang, J., Li, T., Zhang, Y. L., Guo, Z. L., and Xu, L. H. (2011) Effect of microcystin-LR on protein phosphatase 2A and its function in human amniotic epithelial cells. *J. Zhejiang Univ. Sci. B* **12,** 951–960
34. Sandoval, J., Escobar, J., Pereda, J., Sacilotto, N., Rodriguez, J. L., Sabater, L., Aparisi, L., Franco, L., López-Rodas, G., and Sastre, J. (2009) Pentoxifylline prevents loss of PP2A phosphatase activity and recruitment of histone acetyltransferases to proinflammatory genes in acute pancreatitis. *J. Pharmacol. Exp. Ther.* **331,** 609–617
35. Chen, Y., Wang, S., Fu, X., Zhou, W., Hong, W., Zou, D., Li, X., Liu, J., Ran, P., and Li, B. (2015) tert-Butylhydroquinone mobilizes intracellular-bound zinc to stabilize Nrf2 through inhibiting phosphatase activity. *Am. J. Physiol. Cell. Physiol.* **309,** C148–C158
36. Davuluri, G., Gong, W., Yusuff, S., Lorent, K., Muthumani, M., Dolan, A. C., and Pack, M. (2008) Mutation of the zebrafish nucleoporin elys sensitizes tissue progenitors to replication stress. *PLoS Genet.* **4,** e1000240
37. Livak, K. J., and Schmittgen, T. D. (2001) Analysis of relative gene expression data using real-time quantitative PCR and the $2(-\Delta\Delta C(T))$ method. *Methods* **25,** 402–408
38. Detrich, H. W., 3rd, Westerfield, M., and Zon, L.I. (1999) Overview of the zebrafish system. In The Zebrafish: Biology. *Methods Cell Biol.* **59,** 3–10
39. Mullins, M. C., Hammerschmidt, M., Kane, D. A., Odenthal, J., Brand, M., van Eeden, F. J., Furutani-Seiki, M., Granato, M., Haffter, P., Heisenberg, C. P., Jiang, Y. J., Kelsh, R. N., and Nüsslein-Volhard, C. (1996) Genes establishing dorsoventral pattern formation in the zebrafish embryo: the ventral specifying genes. *Development* **123,** 81–93
40. Piccolo, S., Sasai, Y., Lu, B., and De Robertis, E. M. (1996) Dorsoventral patterning in *Xenopus*: inhibition of ventral signals by direct binding of chordin to BMP-4. *Cell* **86,** 589–598
41. Oelgeschläger, M., Larraín, J., Geissert, D., and De Robertis, E. M. (2000) The evolutionarily conserved BMP-binding protein Twisted gastrulation promotes BMP signalling. *Nature* **405,** 757–763
42. Larraín, J., Bachiller, D., Lu, B., Agius, E., Piccolo, S., and De Robertis, E. M. (2000) BMP-binding modules in chordin: a model for signalling regulation in the extracellular space. *Development* **127,** 821–830
43. Branam, A. M., Hoffman, G. G., Pelegri, F., and Greenspan, D. S. (2010) Zebrafish chordin-like and chordin are functionally redundant in regulating patterning of the dorsoventral axis. *Dev. Biol.* **341,** 444–458
44. Dick, A., Hild, M., Bauer, H., Imai, Y., Maifeld, H., Schier, A. F., Talbot, W. S., Bouwmeester, T., and Hammerschmidt, M. (2000) Essential role of Bmp7 (snailhouse) and its prodomain in dorsoventral patterning of the zebrafish embryo. *Development* **127,** 343–354
45. Fürthauer, M., Van Celst, J., Thisse, C., and Thisse, B. (2004) Fgf signalling controls the dorsoventral patterning of the zebrafish embryo. *Development* **131,** 2853–2864
46. Jurynec, M. J., and Grunwald, D. J. (2010) SHIP2, a factor associated with diet-induced obesity and insulin sensitivity, attenuates FGF signaling in vivo. *Dis. Model. Mech.* **3,** 733–742
47. Griffin, K., Patient, R., and Holder, N. (1995) Analysis of FGF function in normal and no tail zebrafish embryos reveals separate mechanisms for formation of the trunk and the tail. *Development* **121,** 2983–2994
48. Sun, Z., Zhao, J., Zhang, Y., and Meng, A. (2006) Sp5l is a mediator of Fgf signals in anteroposterior patterning of the neuroectoderm in zebrafish embryo. *Dev. Dyn.* **235,** 2999–3006
49. Cao, Y., Zhao, J., Sun, Z., Zhao, Z., Postlethwait, J., and Meng, A. (2004) fgf17b, a novel member of Fgf family, helps patterning zebrafish embryos. *Dev. Biol.* **271,** 130–143
50. Logan, C. Y., and Nusse, R. (2004) The wnt signaling pathway in development and disease. *Annu. Rev. Cell Dev. Biol.* **20,** 781–810
51. Chen, C. Y., Chiou, S. H., Huang, C. Y., Jan, C. I., Lin, S. C., Tsai, M. L., and Lo, J. F. (2009) Distinct population of highly malignant cells in a head and neck squamous cell carcinoma cell line established by xenograft model. *J. Biomed. Sci.* **16,** 100
52. Lin, C. W., Liao, M. Y., Lin, W. W., Wang, Y. P., Lu, T. Y., and Wu, H. C. (2012) Epithelial cell adhesion molecule regulates tumor initiation and tumorigenesis via activating reprogramming factors and epithelial-mesenchymal transition gene expression in colon cancer. *J. Biol. Chem.* **287,** 39449–39459
53. Shtutman, M., Zhurinsky, J., Simcha, I., Albanese, C., D'Amico, M., Pestell, R., and Ben-Ze'ev, A. (1999) The cyclin D1 gene is a target of the β-catenin/LEF-1 pathway. *Proc. Natl. Acad. Sci. U.S.A.* **96,** 5522–5527
54. Sherwood, V. (2015) WNT signaling: an emerging mediator of cancer cell metabolism? *Mol. Cell. Biol.* **35,** 2–10
55. Langdon, Y. G., and Mullins, M. C. (2011) Maternal and zygotic control of zebrafish dorsoventral axial patterning. *Annu. Rev. Genet.* **45,** 357–377
56. Lepage, S. E., and Bruce, A. E. (2010) Zebrafish epiboly: mechanics and mechanisms. *Int. J. Dev. Biol.* **54,** 1213–1228
57. Kane, D., and Adams, R. (2002) Life at the edge: epiboly and involution in the zebrafish. *Results Probl. Cell Differ.* **40,** 117–135
58. Schneider, S., Steinbeisser, H., Warga, R. M., and Hausen, P. (1996) β-Catenin translocation into nuclei demarcates the dorsalizing centers in frog and fish embryos. *Mech. Dev.* **57,** 191–198
59. Dougan, S. T., Warga, R. M., Kane, D. A., Schier, A. F., and Talbot, W. S. (2003) The role of the zebrafish nodal-related genes squint and cyclops in patterning of mesendoderm. *Development* **130,** 1837–1851
60. Myers, D. C., Sepich, D. S., and Solnica-Krezel, L. (2002) Bmp activity gradient regulates convergent extension during zebrafish gastrulation.

Dev. Biol. **243,** 81–98
61. Kimelman, D. (2006) Mesoderm induction: from caps to chips. *Nat. Rev. Genet.* **7,** 360–372
62. Beurel, E., Grieco, S. F., and Jope, R. S. (2015) Glycogen synthase kinase-3 (GSK3): regulation, actions, and diseases. *Pharmacol. Ther.* **148,** 114–131
63. Kwon, J., Cho, H. J., Han, S. H., No, J. G., Kwon, J. Y., and Kim, H. (2010) A novel LZAP-binding protein, NLBP, inhibits cell invasion. *J. Biol. Chem.* **285,** 12232–12240
64. Wu, J., Lei, G., Mei, M., Tang, Y., and Li, H. (2010) A novel C53/LZAP-interacting protein regulates stability of C53/LZAP and DDRGK domain-containing protein 1 (DDRGK1) and modulates NF-κB signaling. *J. Biol. Chem.* **285,** 15126–15136